Ubiquitous first-order transitions and site-selective vanishing of the magnetic moment in giant magnetocaloric MnFeSiP alloys detected by Mn 55 NMR

Hussain, R.; Cugini, F.; Baldini, S.; Porcari, G.; Sarzi Amadè, N.; Miao, X. F.; Van Dijk, N. H.; Brück, E.; Solzi, M.; More Authors

DOI
10.1103/PhysRevB.100.104439

Publication date
2019

Document Version
Final published version

Published in
Physical Review B

Ubiquitous first-order transitions and site-selective vanishing of the magnetic moment in giant magnetocaloric MnFeSiP alloys detected by ^{55}Mn NMR

R. Hussain,[1,*] F. Cugini,[1] S. Baldini,[1] G. Porcari,[1] N. Sarzi Amadè,[1] X. F. Miao,[2] N. H. van Dijk,[2] E. Brück,[2] M. Solzi,[1] R. De Renzi,[1] and G. Allodi[1,†]

[1]*Dipartimento di Scienze Matematiche, Fisiche ed Informatiche, Università di Parma, Parco Area delle Scienze 7A, I-43100 Parma, Italy*

[2]*Fundamental Aspects of Materials and Energy (FAME), Faculty of Applied Sciences, Delft University of Technology, Mekelweg 15, 2629 JB Delft, The Netherlands*

(Received 12 April 2019; revised manuscript received 16 August 2019; published 30 September 2019)

We report on a study on a representative set of Fe_2P-based MnFePSi samples by means of ^{55}Mn NMR in both zero and applied magnetic field. The first-order nature of the magnetic transition is demonstrated by truncated order parameter curves with a large value of the local ordered moment at the Curie point, even at compositions where the transition appears second order from magnetic measurements. No weak ferromagnetic order could be detected at Si-poor compositions showing the kinetic arrest phenomenon, but rather the phase separation of fully ferromagnetic domains from volume fractions where Mn spins are fluctuating. The more pronounced decrease of the ordered moment at the $3f$ sites than at the $3g$ sites on approaching T_C, characteristic of the mixed magnetism of these materials, is shown to be driven by the drop of the $3f$ spin density instead of enhanced spin fluctuations. The temperature-driven $3f$ spin extinction is demonstrated to evolve into a truly nonmagnetic state of the $3f$ Mn ions well above T_C, in agreement with theoretical models and in contrast with previous experiments who detected just a partial moment quenching. Besides "normal" $3f$ Mn ions undergoing a magnetic to spinless state transition, NMR in Mn-rich compositions detects the disproportionation at $3f$ sites of a significant minority Mn fraction with negligible hyperfine couplings, which retains its *diamagnetic* character independent of temperature. Such a diamagnetic fraction qualitatively accounts for the reduced average $3f$ moment previously reported at large Mn concentrations.

DOI: 10.1103/PhysRevB.100.104439

I. INTRODUCTION

Magnetic materials showing a first-order magnetic transition (FOMT) have been attracting sustained research interest because of their inherent giant magnetocaloric effect, originating from the large entropy change taking place at the transition. The latter is the key to their employment for magnetic refrigeration, whereby the vapor-based thermodynamic cycles of traditional refrigerators are replaced by magnetization-demagnetization cycles, which are environmentally safer and potentially more efficient. To this end, Fe_2P-based $Mn_xFe_{1.95-x}Si_yP_{1-y}$ alloys ($1 \leqslant x < 1.95$) are among the most promising materials. Their paramagnetic (PM) to ferromagnetic (FM) FOMT is governed by a magnetoelastic transition taking place at the Curie point, characterized by a sizable variation of the crystal cell parameters without a symmetry change. By varying the composition, T_C can be tuned over a wide temperature interval including room temperature, which makes these systems eligible for real case applications.

Like their parent Fe_2P compound, the Mn-Fe-Si-P systems crystallize in the hexagonal space group $P6\bar{2}m$, with a crystal structure characterized by the stacking of $3g$, $1b$ sites and $3f$, $2c$ sites on alternate layers. The magnetic Fe, Mn ions occupy the $3f$ and $3g$ sites, with a marked preference of Mn for $3g$ site [1,2], while the $1b$ and $2c$ sites are occupied by the nonmetallic P and Si ions, with a partial preference of Si for $2c$ sites at $y > 1/3$ [3]. The magnetism of the $3f$ ions exhibits an itinerant character witnessed by a fractional magnetic moment $\leqslant 1.5\ \mu_B$ at low temperature, as compared to $\geqslant 2.5\ \mu_B$ on Mn at the $3g$ sites, which behave as nearly localized spins. The moment at the $3f$ sites exhibits a steep drop at T_C, in coincidence with a marked in-plane lattice contraction, partly compensated by an expansion along c. The accompanying magnetoelastic transition at T_C fits into the scenario of an enhanced chemical bonding of the $3f$ atoms, and increased spin itineracy above the FOMT. The coexistence of large $3g$ Mn moments with weaker and possibly vanishing $3f$ moments is referred to as mixed magnetism. However, the exact nature of the electronic state of the $3f$ ions in the PM state is still controversial. X-ray magnetic circular dichroism (XMCD) experiments indicated, in fact, that the moment quenching above T_C is incomplete, [4] in contrast with earlier predictions for a total $3f$ moment extinction by band-structure calculations [5].

The critical temperature and the character of the magnetoelastic transition are strongly affected by the Mn/Fe and Si/P substitutions. An increasing substitution of P with the larger Si ions at the $2c$ sites gives rise to an in-plane expansion, accompanied by increased $3f$-$3f$ and decreased $3f$-$3g$ minimum distances. In agreement with the tendency observed on crossing the FOMT, this leads to a relative localization of the

*Dipartimento di Fisica, Università di Pavia, Via Bassi 6, I-27100 Pavia, Italy.

†Giuseppe.Allodi@fis.unipr.it

$3f$ moments and an enhanced interlayer exchange coupling, hence a more robust ferromagnetism and an increased T_C are observed. Silicon-poor compositions, on the other hand, yield lower T_C, an unsaturated magnetic moment and strong magnetization hysteresis vs both temperature and applied field. The latter are manifestations of a *kinetically arrested* magnetic transition, i.e., a frozen-in metastable state separated from thermodynamic equilibrium by a large free-energy barrier. The kinetic arrest can, however, be mitigated and eventually suppressed by doping a few percent boron into the $1b$ sites, producing a qualitatively similar, though more dramatic effect as the Si/P substitution. The progressive substitution of Fe by Mn at the $3f$ sites at Mn concentrations $x > 1$, on the other hand, depresses T_C and drives a decrease of the ordered moment [2]. However, the magnetoelastic transition coupled to the FOMT is depressed as well, as witnessed by a smaller step in the lattice parameters. As a consequence, the first-order character of the magnetic transition becomes less pronounced [1,6].

In this paper, we address the study of the magnetic transitions and of mixed magnetism in a representative set of Mn-Fe-Si-P compounds by means of ^{55}Mn nuclear magnetic resonance (NMR). In zero applied field (ZF), ^{55}Mn nuclei resonate in a hyperfine field proportional to the ordered component of the on-site Mn electronic spin and thus provide complementary information to ^{57}Fe Mössbauer spectroscopy [7], with a benefit for NMR due to its simpler spectra. As seen by a local probe of magnetism like ^{55}Mn, a FOMT appears as a *truncated* order parameter curve, [8] i.e., a nonvanishing local moment at the transition temperature, and, rather, a phase-separated magnetic state whereby the volume of the ordered phase vanishes instead. On the other hand, the electronic state of the Mn ion may be detected by the on-site spin density, probed by either the spontaneous hyperfine field at low-temperature or the Knight shift of the resonance line in an applied field in the PM phase. In the mixed magnetism of Mn-Fe-Si-P alloys, in particular, the effect of a decreasing spin polarization on the drop of the $3f$ ordered moment on approaching T_C [2] may be unraveled from that of spin fluctuations, while the evolution to a spinless $3f$ state in the PM phase may be uniquely detected by NMR as a corresponding vanishing of the spin-dependent ^{55}Mn Knight shift [5].

II. EXPERIMENTAL DETAILS

A. Sample preparation and characterization

The Mn-Fe-Si-P(-B) samples were prepared by ball milling for 10 hours of the binary parent Fe_2P compound and high-purity elementary Mn, Fe, red-P, Si (and B, when appropriate), weighed in proper amounts. The resulting fine powder was then pressed into small tablets, sintered for two hours at 1100 °C and annealed for 20 hours at 850 °C in Ar atmosphere, and finally cooled down quickly to room temperature, as detailed elsewhere [1,6,9]. The synthesis was targeted at four compositions representative of different regimes in the magnetic response: $Mn_{1.27}Fe_{0.68}Si_{0.52}P_{0.48}$, $Mn_{1.7}Fe_{0.25}Si_{0.5}P_{0.5}$, $Mn_1Fe_{0.95}Si_{0.29}P_{0.71}$, and $Mn_1Fe_{0.95}Si_{0.33}P_{0.67}B_{0.03}$, referred to hereafter as S1–S4, respectively. Powders from the same batches of samples S2–S4 have also been the subject of the investigations published in Refs. [6,10,11]. The sample homogeneity was assessed by powder x-ray diffraction, revealing a single crystal phase belonging to the appropriate $P6\bar{2}m$ space group.

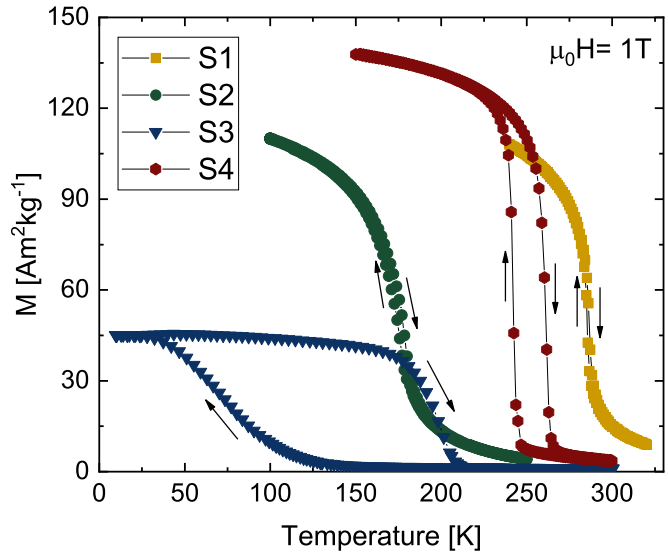

FIG. 1. Magnetization curves vs temperature of the four S1–S4 samples, measured in an applied field of 1 T on both cooling and warming.

The magnetic characterization of the samples was carried out by a superconducting quantum interference device magnetometer (Quantum Design MPMS-XL) in the 2–350 K temperature range and by a MANICS DSM-8 magnetometer equipped with an oven in the 300–800 K range. The magnetization curves of the four samples, recorded as a function of temperature in an applied field of 1 T, are shown in Fig. 1. Sample S1 shows a sharp transition close to room temperature with negligible hysteresis, making this compound of interest for applications. The Mn-richer S2 shows a reduced T_C and a smoother $M(T)$ curve suggesting a second-order magnetic transition (SOMT) in agreement with Refs. [1,6], although a residual hysteresis is also present. The Si-poor S3 exhibits a strong temperature hysteresis and an unsaturated magnetic moment characteristic of a kinetically arrested magnetic state, thoroughly studied by magnetometry and neutron diffraction in Ref. [11]. The full magnetization is recovered and thermal hysteresis is nearly suppressed in S4, similar to S3 but for a slight B doping. The transition temperatures were determined as the inflection points of $M(T)$. In the presence of a distribution of T_C inherent of alloys, due, e.g., to slight local deviations from the nominal stoichiometry unavoidable even in state-of-the-art samples, such a determination is to be intended as the mean T_C. The critical temperatures of the various samples on both warming ($T_C^{\uparrow}$) and cooling ($T_C^{\downarrow}$) are summarized in Table I.

B. NMR experiments

The NMR experiments were carried out by means of a home-built phase-coherent spectrometer [12] and a helium-flow (in the 5–80 K range) or a nitrogen-flow cryostat (70–360 K) on finely powdered samples to maximize the penetration of the radio-frequency (rf) magnetic field.

TABLE I. Composition and critical temperatures of the investigated samples.

Sample	Composition	$T_C^{\uparrow}$ (K)[a]	$T_C^{\downarrow}$ (K)[b]
S1	$Mn_{1.27}Fe_{0.68}Si_{0.52}P_{0.48}$	286.6(2)	285.2(2)
S2	$Mn_{1.7}Fe_{0.25}Si_{0.5}P_{0.5}$	178.5(3)	175.5(3)
S3	$MnFe_{0.95}Si_{0.29}P_{0.71}$	199(1)	73(3)
S4	$MnFe_{0.95}Si_{0.33}P_{0.67}B_{0.03}$	261.7(3)	242(1)

[a]From $M(T)$ on warming (Fig. 1).
[b]From $M(T)$ on cooling (Fig. 1).

Measurements in ZF or in a moderate perturbing magnetic field were performed by using a nonresonant probe circuit, made of a small coil ($\leqslant$50 nH) wound around the sample and terminated onto a 50 Ω resistor. The employment of an untuned probehead allowed, in fact, automated frequency scans, while the sensitivity penalty of a nonresonant circuit was compensated by the rf enhancement of the NMR. The latter consists in the amplification of the NMR signal, due to the hyperfine coupling of nuclear and electronic magnetization, characteristic of ferromagnets [13,14]. The enhancement factor η was estimated as large as $\eta \approx 400$ in ZF, in the typical range of values for nuclei in domain walls, by comparing the excitation conditions in ZF and in a saturating applied field $B_{\rm ext}$, where a much a smaller $\eta \approx B_{hf}/B_{\rm ext}$ in the order of tens is predicted (here B_{hf} is the hyperfine field) [13]. A conventional LC resonator was, however, employed for the weaker $3f$ resonance lines very close to T_C to improve sensitivity, as well as in all the other cases.

The NMR spectra were recorded by means of a standard $P-\tau-P$ spin-echo pulse sequence, with equal rf pulses P of intensity and duration optimized for maximum signal, and delay τ as short as possible, limited by the dead time of the apparatus (in the $2-20\,\mu$s range, depending on the experimental conditions). Each spin echo, representing one frequency point in the spectrum, was analyzed by taking the maximum magnitude of the Fourier-transformed signal, as detailed elsewhere [8], divided by the frequency-dependent sensitivity ($\propto \nu^2$). After such a normalization, the resulting values correspond directly to the spectral distribution of hyperfine fields at the ^{55}Mn nuclei [15].

III. EXPERIMENTAL RESULTS

The ^{55}Mn NMR results in the various experimental or composition regimes are presented for clarity in separate subsections. Each one addresses specific issues: the assignment of the spontaneous ^{55}Mn NMR peaks to corresponding crystal sites and the local moment probed therein, the order of the magnetic transition and the kinetic arrest phenomenon in silicon-poor compounds, the nature of mixed magnetism, and the electronic state at the $3f$ site above T_C, respectively.

A. Mn moment and site occupancy

Very intense spontaneous ^{55}Mn NMR signals were detected below T_C by very low rf excitation power, thanks to the rf enhancement discussed above. The ZF spin-echo amplitudes at low temperature (5 K) are plotted vs frequency ν in Fig. 2 for all our samples. The spectra exhibit two broad peaks with composition-dependent positions and relative weights. The more intense resonance was found in the 260–320 MHz frequency interval (24–30 T in field units), whereas the minority peak, increasing in intensity with increasing Mn concentration, is located in the 150–220 MHz range (14–21 T). Assuming an isotropic hyperfine coupling term in the order of $-11\,{\rm T}/\mu_B$ as in manganites [8] and in other magnetic compounds [16], and neglecting transferred contributions to the contact hyperfine field by neighboring ions, which are known to be very small in these systems, we estimate electronic spin moments of approximately $2.2-2.7\,\mu_B$ and $1.3-1.9\,\mu_B$ at the corresponding Mn sites. These values and the relative amplitudes of the two peaks are in qualitative agreement with the determination of the magnetic moment and the Mn occupancy at the two sites by neutron scattering [2]. The low- and high-frequency ^{55}Mn resonance peaks are therefore unambiguously assigned to Mn nuclei at the $3f$ and $3g$ sites, respectively.

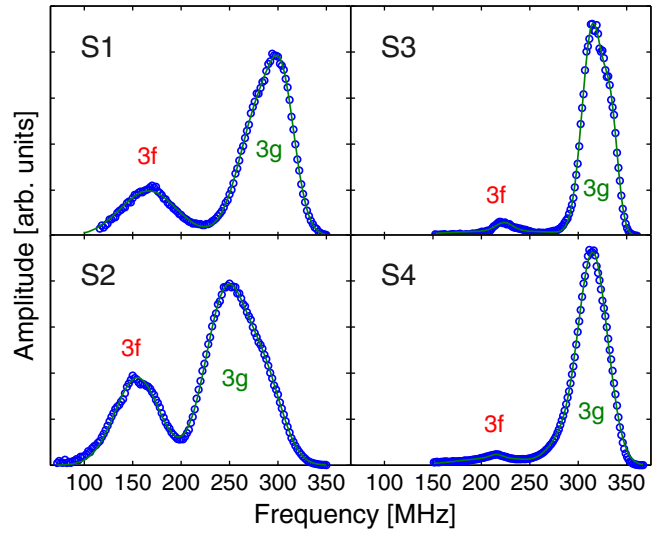

FIG. 2. ZF ^{55}Mn NMR spectra of the S1–S4 samples at $T = 5\,K$.

The best-fit mean frequencies of the two resonance peaks and the ratios of their integrated amplitudes, corresponding to the relative occupancy of the $3f$ and $3g$ sites by Mn, are listed for each sample in Table II. The amplitude ratios are compared with the values expected for a total preference of Mn for the $3g$ site, whereby only Mn atoms in excess of

TABLE II. Low-temperature mean ^{55}Mn ZF-NMR frequencies and relative amplitudes of the main peaks in the spectra of the various samples.

Sample	$\bar{\nu}_{3g}$ (MHz)	$\bar{\nu}_{3f}$ (MHz)	A_{3f}/A_{3g} (measured)	A_{3f}/A_{3g}[a] (expected)
S1	289.4(2)	166.2(2)	0.32(3)	0.27
S2	258.0(2)	154.2(2)	0.50(4)	0.7
S3	320.0(1)	224(1)	0.04(1)	0
S4	312.6(2)	216.2(5)	0.10(2)	0

[a]Assumed equal to $x-1$ (see text).

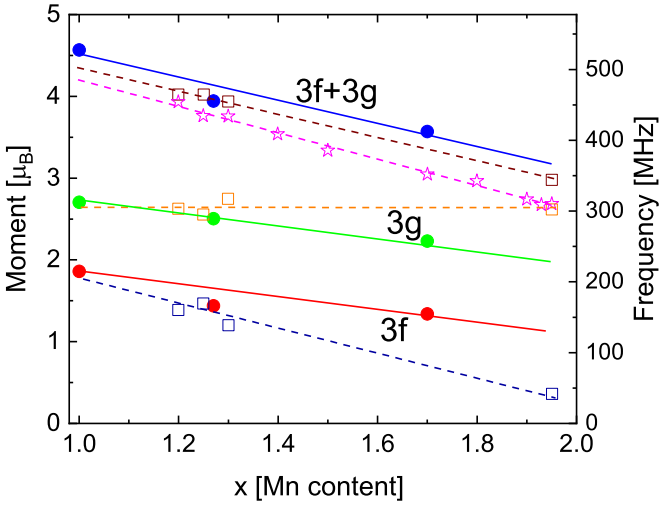

FIG. 3. Low-temperature $3f$, $3g$, and overall ordered moment per FU vs Mn concentration x, determined by neutron scattering (squares) and macroscopic magnetization (stars) in various Mn-Fe-Si-P compounds from the literature [2] compared to the $3f$ and $3g$ ^{55}Mn ZF NMR frequencies and their sum in the present samples (bullets). NMR frequencies are scaled to moments by assuming a $11\,\mathrm{T}/\mu_B$ hyperfine coupling constant.

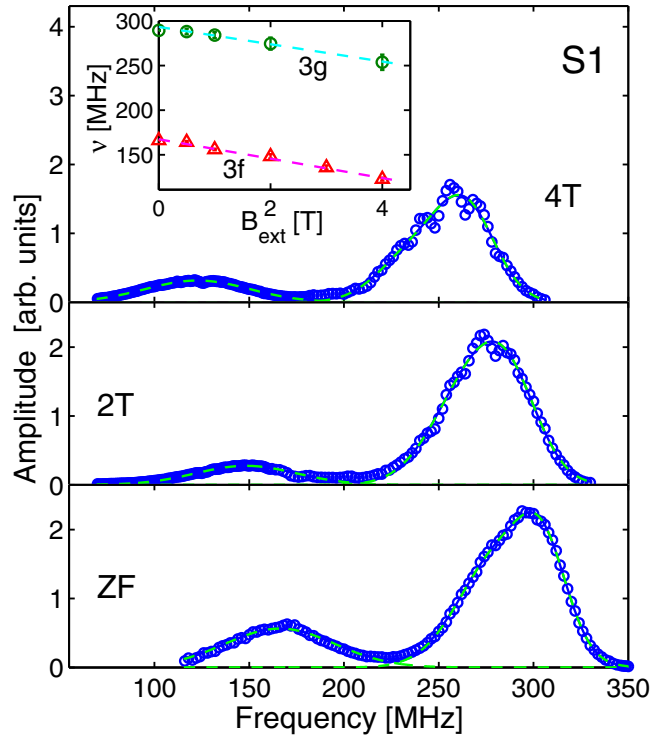

FIG. 4. ^{55}Mn NMR spectra of sample S1 at $T = 5$ K, in zero and in perturbing applied fields. Inset: Mean positions of the $3f$ and $3g$ lines as a function of the external field. The dashed lines are fits to Eq. (1).

1 per formula unit (FU) occupy $3f$ sites. It is apparent from samples S3 and S4 ($x = 1$), showing, however, a small but finite $3f$-Mn fraction, that the preferential occupation of $3g$ sites by Mn is not perfect, and some spillage of Mn and Fe to the disfavored sites occurs. The Mn-rich sample S2 ($x = 1.7$), on the other hand, exhibits a low-moment $3f$-Mn fraction significantly smaller than the expected 0.7 value, a fact that will be commented again in Sec. IV.

The mean spontaneous NMR frequencies of the $3f$ and $3g$ peaks are plotted vs Mn concentration x in Fig. 3, overlaid to the $3f$, $3g$, and overall moment per FU determined by neutron scattering, and to the macroscopic saturation moment per FU reported in the literature for similar compounds [2]. In the figure, NMR frequencies are scaled to moments by assuming a mean hyperfine field of $11\,\mathrm{T}/\mu_B$, as stated above. The total moment $\mu_{3g} + \mu_{3f}$ assessed by ^{55}Mn ZF-NMR is in good agreement with its determinations by the other techniques. The agreement of the $\bar{\nu}_{3g}$ and $\bar{\nu}_{3f}$ NMR frequencies with the individual $3g$ and $3f$ moment values refined by neutrons is, however, poorer. In particular, NMR shows a similar relative decrease with increasing x for the $\bar{\nu}_{3g}$ and $\bar{\nu}_{3f}$ resonance frequencies, while a constant μ_{3g} and a more rapidly decreasing μ_{3f} moment were estimated from neutron data.

The attribution of both the resonance peaks to ^{55}Mn nuclei (rather than ^{31}P, which also experience a large transferred hyperfine field in the parent Fe_2P compound) [17] is further demonstrated by the application of moderate external fields acting as a perturbation of the much larger internal field. Typical spectra in external fields up to a few tesla are shown in Fig. 4 for a representative sample (S1). Both the $3g$ and $3f$ mean resonance frequencies shift to lower frequency following a linear dependence on the the applied field,

$$\bar{\nu}_\alpha(H) = \frac{\gamma}{2\pi}\left|B_{hf}^{(\alpha)} + \mu_0 H\right| = \frac{\gamma}{2\pi}\left(\left|B_{hf}^{(\alpha)}\right| - \mu_0 H\right), \qquad (1)$$

($\alpha = 3g, 3f$), where $B_{hf}^{(\alpha)}$ is the isotropic component of the hyperfine field and $\gamma/2\pi = 10.5$ MHz/T is the gyromagnetic ratio of ^{55}Mn (figure inset). The collinear composition of the isotropic hyperfine field (collinear in turn to the on-site electronic moment) and the external field is demonstrated by the shift with an absolute rate $\mu_0^{-1}|d\bar{\nu}_\alpha/dH|$ equal to the full ^{55}Mn gyromagnetic ratio $\gamma/2\pi$, without line splitting or appreciable broadening. The negative sign of $d\nu_\alpha/dH$ indicates that the hyperfine field is antiparallel to the electronic spin, in agreement with the core-polarization mechanism dominant in the contact hyperfine coupling of transition metal ions [18]. All these facts prove, therefore, the full FM order of both sublattices.

Similar field-dependent spectra were recorded in all samples. In particular, they were detected also in the kinetically arrested S3, which shows a $M(H)$ curve saturating in two steps [Fig. 2(b) of Ref. [11]], with the full saturation taking place in a field H_s as high as $\mu_0 H_s \approx 5$ T, and a large hysteresis in $M(H)$ below H_s. The field dependence of the mean frequency $\bar{\nu}_{3g}$ of the majority peak is plotted vs field in the inset of Fig. 5, overlaid to a plot of the $\nu(H)$ law of Eq. (1). It is apparent from the figure that, above an external field of 2 T corresponding to the saturation of the magnetically ordered domains, the collinear composition of the internal with the external field as of Eq. (1) is obeyed by $\bar{\nu}_{3g}(H)$. The local magnetic order probed by NMR is therefore fully FM in sample S3 as well. In the main panel of Fig. 5, two low-temperature spectra are compared, recorded in the same field $\mu_0 H = 1\,\mathrm{T} < \mu_0 H_s$ applied after zero-field cooling (ZFC) and after an isothermal field ramp up to H_s followed

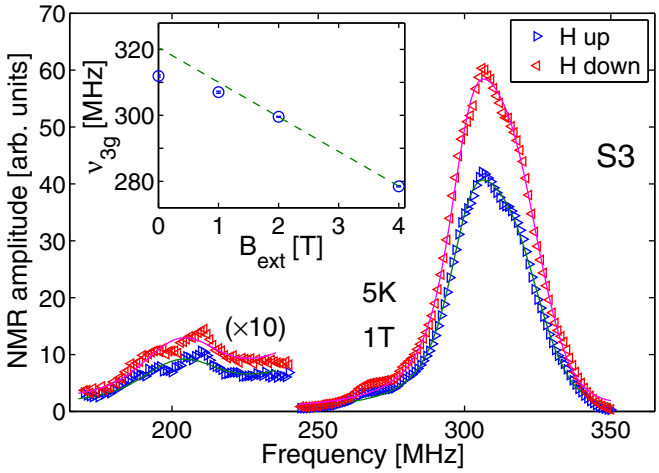

FIG. 5. ^{55}Mn NMR spectra of sample S3 at $T = 5$ K in an applied field $B_{\rm ext} = 1$ T, applied after ZFC to the working temperature (blue right triangles) and after ZFC to 5 K, followed by an isothermal field cycle $0 \rightarrow 5\,{\rm T} \rightarrow 1\,{\rm T}$ (red left triangles). Inset: Mean position $\bar{\nu}_{3g}$ of the $3g$ line vs $B_{\rm ext}$. The dashed line is a fit of the two highest-field points $\bar{\nu}_{3g}(B_{\rm ext})$ to Eq. (1), with γ constrained to the ^{55}Mn value.

by a ramp down to the measuring field, respectively. Clearly, only the signal amplitude is hysteretic vs field cycles, while the spectra are identical but for a vertical scaling relative to each other. This indicates that the microscopic properties of the magnetically ordered phase are unaffected by the applied fields, and only its volume is increased.

B. First-order transitions and kinetic arrest

The ZF ^{55}Mn NMR spectra could be recorded up to T_C in all samples. The temperature dependence of the centers of gravity $\bar{\nu}_{3g}$ and $\bar{\nu}_{3f}$ of the two resonance peaks, proportional

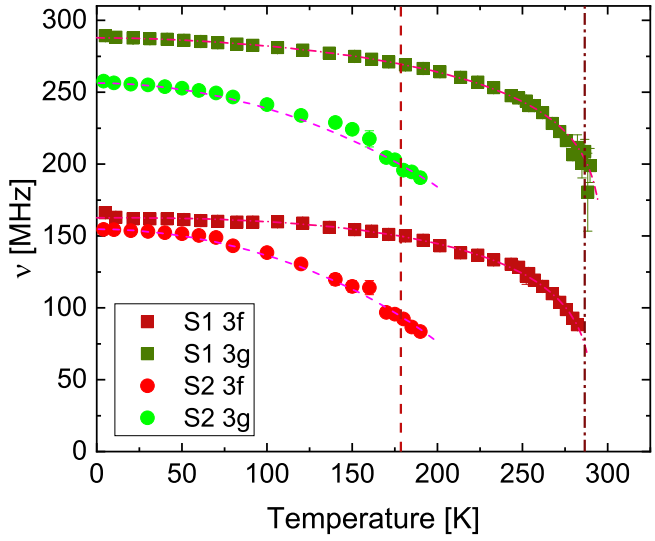

FIG. 6. ZF $3g$ and $3f$ mean ^{55}Mn resonance frequencies vs temperature, recorded on warming in samples S1 (squares) and S2 (bullets). The lines overlaid to symbols are guides to the eye. Vertical dashed lines mark the upper transition temperatures $T_C^{\uparrow}$ of the two samples.

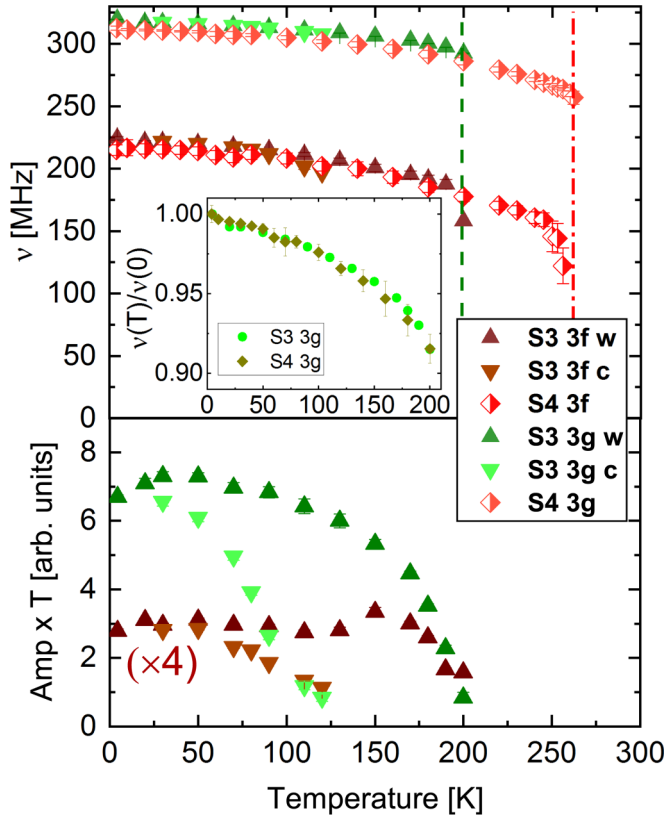

FIG. 7. Top: ZF $3g$ and $3f$ mean ^{55}Mn resonance frequencies vs temperature of samples S3 on cooling (point-down triangles) and warming (point-up triangles), and of S4 on warming (diamonds). The upper transition temperatures $T_C^{\uparrow}$ of the two samples are marked by vertical dashed line. Inset: Normalized $3g$ resonance frequencies $\bar{\nu}_{3g}(T)/\bar{\nu}_{3g}(0)$ vs T of the two samples. Bottom: Integrated $3f$ and $3g$ peak amplitudes times temperature T, as a function of T. For clarity, the $3f$ data are scaled by a vertical factor of 4.

to the mean local moments at the two Mn sites, is plotted in Figs. 6 and 7 for samples S1–S2 and S3–S4, respectively. In the figures, the warming-up higher transition temperatures $T_C^{\uparrow}$ of Table I are marked by vertical dashed lines for reference. It is apparent from the figures that the $\bar{\nu}_{3g}(T)$ order parameter curves do not vanish at T_C in any sample. The reduced order parameter at the $3g$ site $\bar{\nu}_{3g}(T)/\bar{\nu}_{3g}(0)$ is approximately 0.8 at T_C and extrapolates to zero at a significantly higher temperature. This holds true also for sample S2, showing a comparatively small thermal hysteresis and a magnetization vs temperature dependence resembling that of a SOMT (Fig. 1). These *truncated* order parameter curves (i.e., not vanishing at T_C), as seen by a local probe in direct space like NMR, indicate that the magnetically ordered phase does not collapse on warming due to critical spin fluctuations but, rather, to an independent mechanism which abruptly breaks down magnetic order. The truncation effect is therefore a clear indication of a FOMT.

To reconcile the seeming SOMT from magnetization data in sample S2 with the marked first-order character apparent from ^{55}Mn NMR, it is worth noting that spontaneous ^{55}Mn resonances are detected in this sample several kelvin above T_C without noticeable anomalies in $\bar{\nu}_{3g}(T)$ and $\bar{\nu}_{3f}(T)$ (Fig. 6).

This behavior indicates the coexistence of a FM and a PM phase over a wide temperature interval across the transition, with the FM fraction surviving above T_C as a minority phase. Therefore, it is the volume fraction of the ordered phase which tends continuously to zero on warming.

The $3g$ and $3f$ order parameter curves of sample S3, showing a marked thermal hysteresis and the kinetic arrest phenomenon, are plotted vs temperature on both cooling and warming in Fig. 7 (top panel). Very small and negligibly small differences in the values of $\bar{\nu}_{3f}$ and $\bar{\nu}_{3g}$, respectively, are detected between the cooling and warming scans, and only close to the lower transition $T_C^{\downarrow}$. In the figure, $\bar{\nu}_{3g}(T)$ and $\bar{\nu}_{3f}(T)$ of S3 are overlaid to the corresponding quantities of sample S4, containing the same nominal amount of Mn but showing in contrast higher T_C, a much narrower hysteresis and the full saturation moment. Notably, the spontaneous NMR frequencies of the two samples follow the same relative dependence of temperature and can be made to overlap by a vertical scaling factor of $\approx$1.02 (figure inset). The near coincidence of the $\bar{\nu}$ absolute values in these macroscopically very different samples is in essential agreement with the reported finding that the local $3g$ and $3f$ moments depend to leading order only on Mn content [2,3,19].

The integrals of the NMR signal amplitude of S3 over the $3g$ and $3f$ peaks, normalized by the Boltzmann factor $1/T$, are plotted vs T in the bottom panel of Fig. 7. Where the signal loss due to the spin-spin nuclear relaxation is negligible, i.e., far enough from $T_C^{\uparrow}$, the plotted quantities are proportional to the number of resonating nuclei, hence to volume of the ordered phase. In contrast to $\bar{\nu}_{3f}(T)$ and $\bar{\nu}_{3g}(T)$, the normalized signal amplitude is strongly hysteretic vs T, and its temperature behavior closely reproduces that of $M(T)$. The thermal hysteresis of the magnetically ordered volume is therefore qualitatively similar to the isothermal hysteresis vs H shown above. Notably, a spin-density wave (SDW), identified with the competing phase to the FM one, was reported in this sample by neutron scattering across T_C [11]. No NMR signal component distinct from the two-peak spectrum of Fig. 2(c), however, could be detected down to the lowest temperatures. Although the detection of a SDW might be hindered by a diminished sensitivity of NMR to ^{55}Mn nuclei in non-FM phases, due to a smaller rf enhancement therein [13,14], we deem unlikely that the missing SDW signal is solely due to this reason. Actually, moderately large enhancement factors may indeed be found also in antiferromagnets and weak ferromagnets [14,20,21], unless they are magnetically very hard. More plausibly, the discrepancy between the findings of NMR and neutrons is due to the much longer timescale of the former, as will be discussed in Sec. IV.

C. Mixed magnetism

A careful examination of $\bar{\nu}_{3g}(T)$ and $\bar{\nu}_{3f}(T)$ in the various samples reveals that the two quantities, probing the ordered Mn moments at the $3g$ and the $3f$ sites, do not scale with each other as a function of temperature and seemingly behave as independent order parameters. In particular, $\bar{\nu}_{3f}(T)$ decreases faster than $\bar{\nu}_{3g}(T)$ on warming. This is apparent from Fig. 8, showing a continuous increase of the $\bar{\nu}_{3g}(T)/\bar{\nu}_{3f}(T)$ ratio with temperature in all four samples and a clear upturn at T_C in

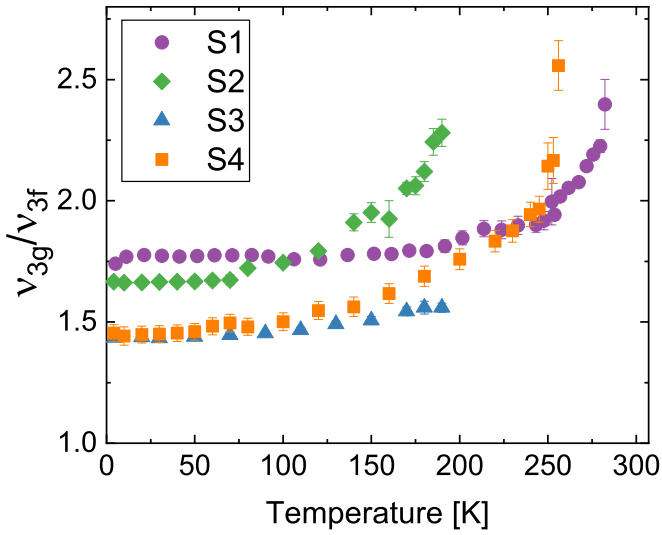

FIG. 8. Mean frequency ratio $\bar{\nu}_{3g}/\bar{\nu}_{3f}$ of the $3g$ and $3f$ ZF ^{55}Mn NMR peaks in the four samples, as a function of temperature.

samples S1, S2, and S4. The steeper temperature dependence of the $3f$ ordered moment on approaching T_C, in agreement with previous reports by other techniques [2,4,5], is a clear manifestation of the weaker magnetism of the $3f$ ion, possibly evolving into a nonmagnetic state. Its coexistence with the larger and more localized $3g$ moment is referred to altogether as *mixed magnetism*, and it is believed to play an important role in the FOMTs of this class of materials [6,10,11,22]. Nevertheless, it is clear from Figs. 6 and 7 that also $\nu_{3f}(T)$, with the sole possible exception of sample S1, maintains a finite value at T_C, as in a truncated order parameter curve. This is particularly evident in the kinetically arrested S3 sample, showing just a moderate increase with temperature in $\bar{\nu}_{3g}(T)/\bar{\nu}_{3f}(T)$ (Fig. 8). It seems, therefore, that the FOMT and the drop of the $3f$ moment are partly independent phenomena.

The nature of the observed drop of the $3f$ *ordered* moment on approaching T_C is demonstrated by nuclear relaxations. Spin-spin relaxation rates T_2^{-1}, measured in ZF on the two resonance peaks, are plotted vs temperature in Fig. 9 for a representative sample (S1). Far enough from T_C, T_2^{-1} is smaller at the $3f$ than at the $3g$ site by a factor of 2, in qualitative agreement with the smaller hyperfine coupling of $3f$ ions, on which relaxation rates depend quadratically. The quantitative discrepancy with the $(\bar{\nu}_{3g}/\bar{\nu}_{3f})^2 \approx 3$ value expected from the isotropic hyperfine couplings of the two sites is possibly accounted for by anisotropic couplings, which also produce nuclear relaxations without a net effect on the mean resonance frequencies, and which are comparable for the two peaks as indicated by their similar absolute linewidths. Nevertheless, the ratio of T_2^{-1} at the $3g$ over the $3f$ site increases on warming. This rules out enhanced spin fluctuations (due, e.g., to weakened exchange interactions) as the origin for the loss of the $3f$ ordered moment, as the latter would lead to relatively stronger nuclear relaxations on the $3f$ peak, contrary to evidence. The $3f$ moment drop is therefore due to the decrease of the spin polarization and the tendency to a

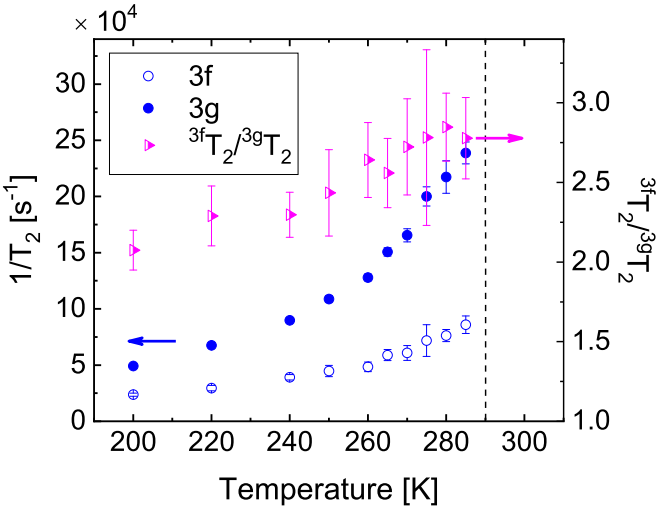

FIG. 9. Spin-spin ^{55}Mn relaxation rates of sample S1, measured in ZF on the $3g$ (filled circles) and $3f$ peak (empty circles) as a function of temperature, and their ratios (triangles).

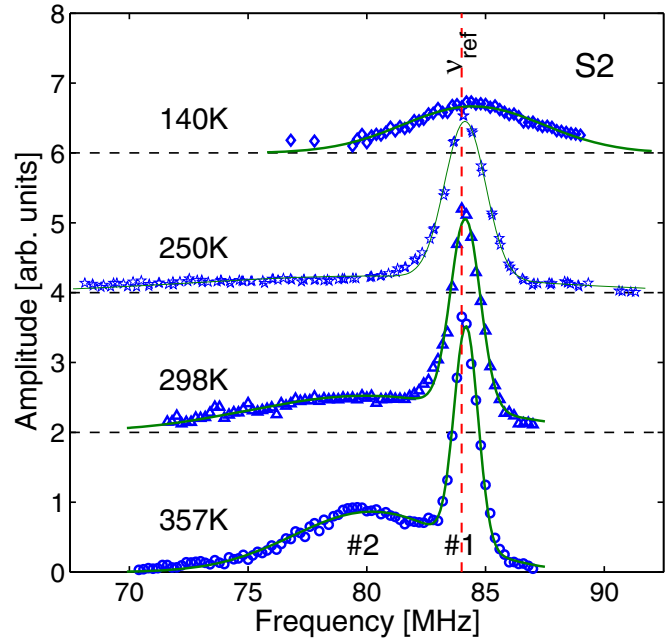

FIG. 10. ^{55}Mn NMR spectra of sample S2 in an applied field of 7.96 T (^{55}Mn reference frequency $\nu_{\rm ref} = 83.998$ MHz) at several temperatures.

nonmagnetic state of the $3f$ ions, in agreement with XMCD experiments and band calculations [4,5].

D. Vanishing $3f$ moment and diamagnetic Mn

The PM phase at temperatures well above T_C was investigated in an applied field $B_{\rm ext} = 7.96$ T mostly in sample S2, featuring both a large $3f$ fraction and relatively low T_C which matches the temperature range of our N_2-flow cryostat. In such experimental conditions, NMR can only probe nonmagnetic or weakly magnetic Mn species. The signal of ^{55}Mn nuclei of a PM ion like $3g$ Mn, experiencing a fluctuating hyperfine field in the order of 25 T, would relax with relaxation times $T_2 \ll 1\,\mu$s [23,24], i.e., much shorter than the dead time of a pulsed NMR receiver, and therefore it cannot be detected.

A set of ^{55}Mn NMR spectra recorded at several temperatures above T_C is shown in Fig. 10. The highest temperature spectrum (357 K) consists of two well-resolved resonance peaks: a sharper line with a small positive shift with respect to the ^{55}Mn reference (83.998 MHz), referred to hereafter as line 1, and a much broader resonance with a negative shift $K \approx -4.5\%$ (-4 MHz in absolute units), referred to as peak 2. The two peaks, whose intensity is not corrected for spin-spin relaxations in the plot, exhibit comparable raw integrated amplitudes. However, the recorded signal amplitude of line 2 is decayed by a factor of 4 from the initial value due to a transverse relaxation time $T_2 = 12(1)\,\mu$s shorter than the duration of the spin-echo pulse sequence employed to excite the resonance, while the signal loss of line 1 due to relaxation ($T_2 = 85(1)\,\mu$s), on the contrary, is negligible. Therefore, line 1 originates from a minority fraction of nuclei.

The evolution of the ^{55}Mn NMR spectrum on cooling down to 250 K, a temperature still well above T_C, is summarized by Fig. 11, showing the shifts $K(T)$ (panel a) and widths $\sigma(T)$ (c) of the two lines as a function of temperature. The spin lattice relaxation rates $T_1^{-1}(T)$ are also plotted in Fig. 11(a), overlaid to the $K(T)$ data. On both peaks, they obey the Korringa law $T_1^{-1} \propto T$ typical of metals [25,26], as is apparent from Fig. 11(b), showing Korringa products $T_1^{-1}T^{-1}$ independent of T within experimental accuracy. The T_1^{-1} rates of peak 2 are larger than on peak 1 by approximately a factor of 7, in agreement with a similar ratio observed in T_2^{-1} (see above). This indicates that ^{55}Mn nuclei in the former experience stronger interactions with electronic spins. The same conclusion is supported by the Gaussian linewidths of the two peaks, originating from the anisotropic interactions of nuclei (dipolar and anisotropic hyperfine) with the surrounding static moments. The temperature dependence of the Gaussian linewidth $\sigma_2(T)$ of peak 2 mimics that of the magnetic susceptibility $\chi(T)$ [overlaid to the $\sigma(T)$ data of Fig. 11(c) for reference], while its magnitude largely exceeds the contribution from static dipolar fields at the $3f$ site, for which a limiting value of approximately 2 MHz is calculated in the FM phase. These two features demonstrate therefore a sizable *anisotropic* hyperfine coupling term for the corresponding nuclei.

The isotropic hyperfine contact term proportional to the on-site spin density, on the other hand, is probed by the line shift $K(T)$ after the subtraction of possible temperature-independent chemical (i.e., orbital) shift terms. Figure 11(a) clearly shows that the sizable shift $K_2(T)$ of line 2 is nearly independent of temperature, and it is therefore dominated by a chemical shift in the order of -4%. Such a large value is comparable to those reported for nuclei of transition metal ions in their nonmagnetic ground state, like, e.g., low-spin cobalt [27], and it demonstrates its origin from low-lying excited crystal field states via the van Vleck mechanism [28]. The isotropic hyperfine coupling of these ^{55}Mn nuclei, probed by the residual temperature-dependent component of $K_2(T)$, can

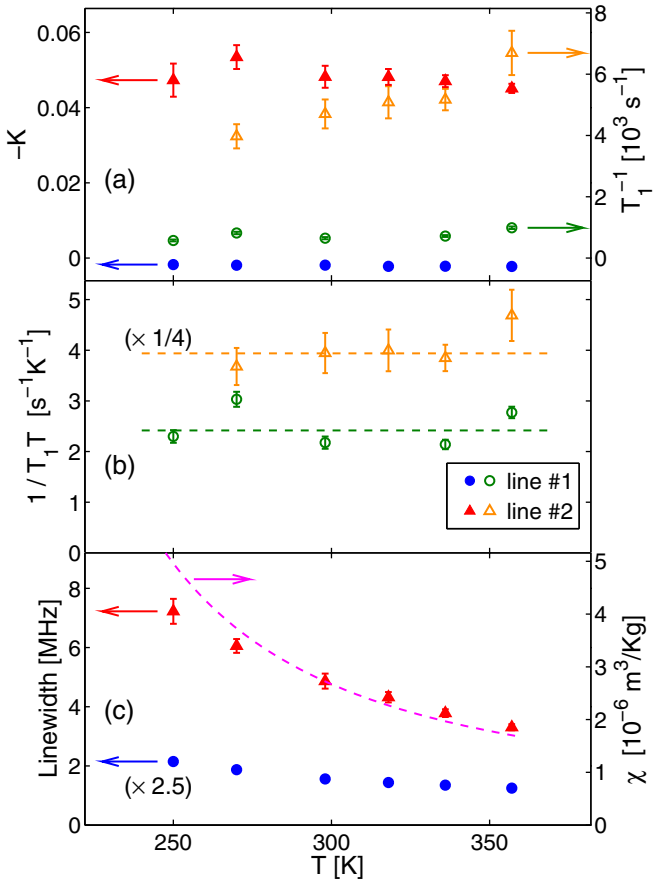

FIG. 11. Top: Reverse-sign line shifts (filled symbols) and spin-lattice relations T_1^{-1} (open symbols) as a function of temperature for the two resonance lines in the ^{55}Mn NMR spectra of sample S2 in the PM phase (Fig. 10). Middle: Korringa product $T_1^{-1}T^{-1}$ vs T for the two ^{55}Mn resonance lines. For clarity, the plotted values of line 2 are divided by a constant ratio of 4. Bottom: Gaussian NMR linewidths σ vs T of the two ^{55}Mn resonance lines (symbols) and DC susceptibility measured in $\mu_0 H = 1$ T (line). For clarity, the $\sigma(T)$ data of the narrower line 1 are magnified by a constant factor of 2.5 in the plot.

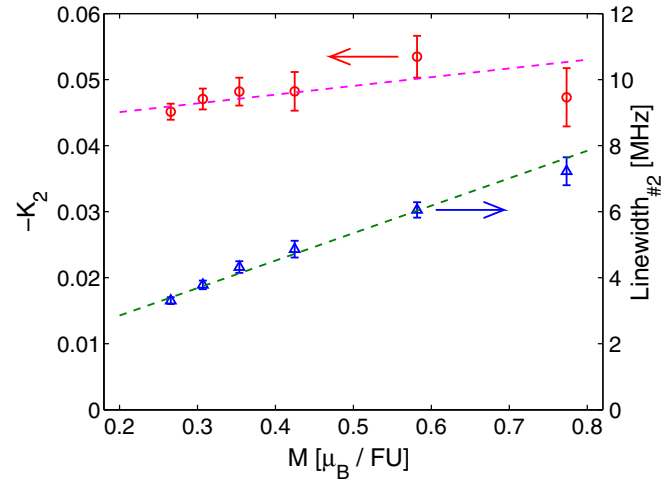

FIG. 12. Negative lineshift $-K_2$ and linewidth σ_2 of line 2 in the ^{55}Mn NMR spectra of sample S2 of Fig. 10, plotted as a function of the macroscopic magnetic moment calculated from the $\chi(T)$ data of Fig. 11(c).

be better estimated by comparison with magnetometry data in the K vs M plot of Fig. 12, where temperature is the implicit parameter. The linear fit in the figure extrapolates to a maximal spin-dependent component in $\Delta K_2^{(\mathrm{sat})} = (\partial K_2/\partial M)M_s = -0.04(2)$ for a saturation moment $M_s \approx 3\mu_B$ per FU, i.e., a hyperfine field $B_{hf}^{(\mathrm{iso})} = \Delta K_2^{(\mathrm{sat})} B_{\mathrm{ext}} = -300 \pm 150$ mT in the virtual magnetically saturated state which would be attained in an infinite applied field. Assuming an on-site origin for the electronic polarization at the nucleus, the latter corresponds to a saturation Mn moment of just $\approx 0.03\,\mu_B$, according to the core-polarization coupling constant of about 11 T/μ_B demonstrated above by comparing NMR with neutron scattering data. For reference, the extrapolation from the analogous linear dependence of σ_2 on M (shown in Fig. 12 as well) yields an asymptotic linewidth $\sigma_2^{(\mathrm{sat})} = 25(2)$ MHz, whence a rms anisotropic hyperfine field $B_{hf}^{(\mathrm{anis})} = \sqrt{3}\,\sigma_2^{(\mathrm{sat})} 2\pi/\gamma = 4.1(3)$ T [29]. Such a large value of $B_{hf}^{(\mathrm{anis})}$ cannot arise from the tiny on-site spin moment estimated above [30] and therefore must be a transferred contribution from neighboring magnetic ions. Given the presence of a large, though anisotropic, transferred hyperfine field at the corresponding Mn site, a transferred origin cannot be ruled out for its much smaller $B_{hf}^{(\mathrm{iso})}$ as well. Therefore, this majority ^{55}Mn NMR signal is compatible with a strictly spinless Mn species. In view of the mixed magnetism detected in these materials by several techniques, including the ZF ^{55}Mn NMR experiments on this exact sample reported in this paper, this resonance is undoubtedly assigned to Mn ions at $3f$ sites.

We now focus on the sharper line 1, arising from a minority Mn fraction, as commented above. It is apparent from Figs. 10 and 11(a) that its shift K_1, much smaller than K_2 and opposite in sign, is practically independent of temperature. Moreover, the magnitude of its linewidth $\sigma_1(T)$, also much smaller than $\sigma_2(T)$, agrees with a dominant dipolar origin from neighboring classical electronic moments, hence with a very small spin polarization of the local wave function. These two facts indicate, respectively, vanishing isotropic and a small anisotropic hyperfine couplings, i.e., a *diamagnetic* behavior. Indeed, this Mn species does not develop a magnetic ground state on cooling, unlike the majority fraction probed by peak 2, as witnessed by the detection of the corresponding resonance safely below T_C, broadened ($\sigma_1 \approx 3$ MHz at $T = 140$ K), but essentially unshifted (Fig. 10). Though a minority diamagnetic Mn fraction, however, its belonging to a nonmagnetic impurity phase can be safely ruled out. Its amount is estimated in fact as large as 0.12(2) atoms per FU from the amplitude of its ^{55}Mn NMR peak relative to peak 2 probing $3f$ Mn (see above), and the assessment of $3f$ Mn abundance from low-T ZF NMR (Table II). This figure is also supported by its comparison with the intensity of ^{31}P nuclear resonance in this sample, yielding the same estimate [31]. A spurious phase in such an amount would have been detected by x-ray diffraction, contrary to experimental evidence. Moreover, its nuclear relaxations are only moderately weaker than on peak 2 and in the typical range of nuclei of nonmagnetic ions in magnetic materials, like, e.g., ^{139}La in lanthanum manganites

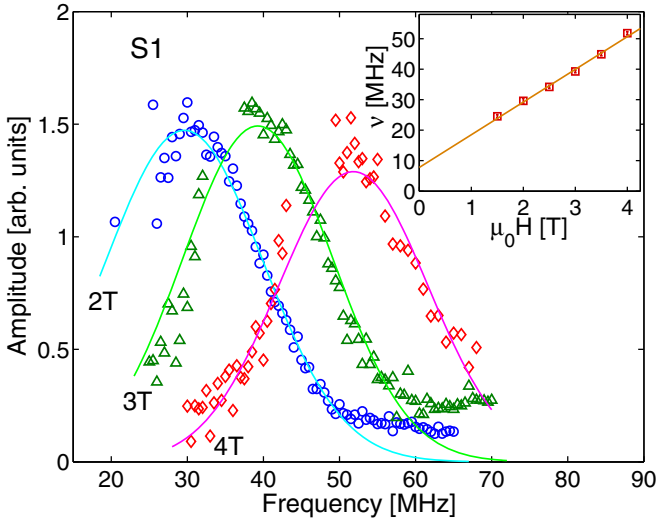

FIG. 13. ^{55}Mn NMR resonance lines from the diamagnetic Mn fraction of sample S1 at $T = 5$ K, in various applied fields. Inset: Mean resonance frequency $\bar{\nu}$ vs applied field.

[32,33] and cobaltates [27]. This proves that these nuclei experience electronic spin fluctuations and therefore belong to the proper MnFeSiP phase.

An indication on the origin of this so-called diamagnetic Mn fraction is provided by its systematic search in the other samples. Resonances perfectly similar to lines 1 and 2, except for a larger chemical shift of the former ($K_1 \approx 1.3\%$) and overall broader spectra due the vicinity of T_C, were also found in sample S1 above 290 K up to he highest available temperature (360 K) [34]. The origin of the sharper line from diamagnetic Mn atoms, which retain their nonmagnetic character down to the lowest temperature, is confirmed by the ^{55}Mn resonance peaks detected at $T = 5$ K in the frequency scans of Fig. 13 in moderate applied fields (so the corresponding frequency intervals are disjoint from the field-shifted $3f$ spontaneous resonance). The common origin of these low-temperature signals with the high-temperature line 1 is proven by their shift with field according to the ^{55}Mn gyromagnetic ratio γ (times a small correction for the chemical shift K_1) and a small positive internal field $B_{hf} = 0.7$ T, in agreement with the relation

$$\bar{\nu}(H) = \frac{\gamma}{2\pi}[B_{hf} + \mu_0(1 + K_1)H] \qquad (2)$$

(see Fig. 13 inset). The positive sign of B_{hf}, in contrast with the negative spin hyperfine coupling of transition metal ions arising from core polarization, in fact warrants its transferred origin, compatibly with a spinless Mn state.

The search for signals from nonmagnetic Mn at both room and low temperature, on the contrary, was unsuccessful in samples S3 and S4. Based on the estimated sensitivity of our NMR measurements, the missed detection of such signals poses an upper limit to a possible diamagnetic Mn fraction not exceeding 0.01 Mn atoms per FU. Its practical absence in these two Mn-poor samples, incidentally with a small, if not vanishing, concentration of Mn atoms at the $3f$ sites (Tables I and II), as opposed to its sizable amount found in the Mn-richer S1 and S2 samples, suggests that also diamagnetic Mn atoms are located at $3f$ sites.

IV. DISCUSSION

The nonvanishing magnetic order parameter at T_C, probed locally by the spontaneous ^{55}Mn resonance frequency $\bar{\nu}_{3g}(T)$ at the $3g$ site, proves that the magnetic transition of Fe_2P-based Mn-Fe-Si-P alloys is strongly first order in all the investigated compositions. The abrupt drop of the net macroscopic moment on warming at a transition temperature T_C at which the local moment is still relatively large, indicates in fact that magnetic order collapses due to the breakdown of exchange coupling. Similar FOMTs, detected from truncated precession frequency [8,35] or spin-wave stiffness curves [36], have been observed, e.g., in double-exchange manganites and ascribed therein to the disruption of the half-metallic state and the onset of a polaron phase. In the present materials, the driving mechanism for the FOMT is known to reside in the concomitant magnetoelastic transition at T_C. ZF ^{55}Mn NMR demonstrates the first-order character of the transition, in particular, also at a Mn concentration as high as $x = 1.7$ (sample S2), where a SOMT was formerly inferred from a smoother $M(T)$ magnetization curve and a shallower magnetic entropy peak at the transition [1,6]. Nevertheless, at this composition, the truncation effect on the order parameter curve $\bar{\nu}_{3g}(T)$ is as severe as at other compositions. The seeming discrepancy between the results from NMR and macroscopic techniques can, however, be reconciled by taking into account that the magnetic transition in this compound is characterized by a PM-FM phase coexistence over a wide temperature interval, as already pointed out above. The latter indicates a broad distribution of T_C in the material, arising from a corresponding broad distribution of critical temperatures for the driving magnetoelastic transition. This interpretation is actually corroborated by x-ray diffraction data, showing a smoother variation of the lattice parameters in this sample, as compared to the steplike jump observed in the other ones [6]. Therefore, although the overall effect of such inhomogeneities on the macroscopic magnetism accidentally mimics a SOMT, it is clear that here the continuous parameter at T_C is the ordered volume instead of the local moment, and that this magnetic transition is not driven by critical fluctuations. Based on this finding for this compound, whose macroscopic response shows the closest resemblance to that of a SOMT, we conclude that no real SOMT can be found in the composition phase diagram of Mn-Fe-Si-P alloys, and therefore FOMTs are a general property of these materials.

A similar spatial segregation of the FM phase from a non-FM one, rather than a weak FM structure, is identified by NMR in the kinetically arrested magnetic order of the Si-poor S3 compound, apparent from its unsaturated and strongly hysteretic magnetization. The ^{55}Mn NMR spectra in fact show hysteretic amplitude and nonhysteretic shape vs temperature and applied magnetic field (Figs. 5 and 7), as well as the parallel alignment of Mn spins to an applied magnetic field. This demonstrates that the macroscopic magnetic moment develops by the nucleation of fully FM domains whose inner electronic and magnetic properties are unaffected by thermal and field cycles, while only the magnetically

ordered volume is hysteretic vs both temperature and applied field. The competing phase to the FM fraction, identified by neutron scattering with an incommensurate SDW [11], was not, however, detected by our experiments. The reason for the missed detection of a SDW by NMR most likely relies on the comparatively longer timescale of our technique. Two possible cases may be envisaged, each one posing a different limit to the characteristic time τ_c of the spin dynamics in the SDW. The spin-density modulation might be entirely dynamic in nature and indistinguishable from the PM phase over the time window of an NMR experiment, a hypothesis setting an upper limit $\tau_c \leqslant 10^{-5}$ s to its correlation time. Even though, on the contrary, the SDW is mostly static, it might be subject to sizable and relatively slow spin or charge excitations, similar to those reported in manganites [33] and in layered cobaltates. [27] Under reasonable assumptions about the coupling of such excitations to ^{55}Mn nuclei, the NMR signal would be lost due to exceedingly fast relaxations in the case of $\tau_c \geqslant 10^{-9}$ s.

The mixed magnetism of the Mn-Fe-Si-P systems is detected by ZF NMR through distinct temperature dependencies of the ordered moments at the $3f$ and $3g$ sites. The steeper decrease of the $\bar{\nu}_{3g}$ NMR order parameter on warming up to T_C, not accompanied by excess spin fluctuations which would produce stronger nuclear relaxations on the $3f$ peak, contrary to experimental evidence (Fig. 9), demonstrate the drop of the spin polarization at the $3f$ site and not just its ordered component. Its extinction develops as a progressive reduction over a wide temperature range on warming and it is still incomplete at T_C, as it is apparent by the non-zero $\bar{\nu}_{3g}(T_C)$ value (sample S1, featuring the highest T_C, is a possible exception to the latter behavior). This suggests that the FOMT in these materials, though related to the weakening of the $3f$ magnetism observed with increasing temperature, is not simply triggered by the vanishing of the $3f$ moment. This is particularly evident in the kinetically arrested S3 compound, showing only a moderate reduction of the $3f$ moment at its upper transition temperature $T_C^{\uparrow}$. Notably, the mean hyperfine frequencies $\bar{\nu}_{3g}(T)$, $\bar{\nu}_{3f}(T)$ *of both lines* of S3 closely follow those of the S4 compound, similar but for slight boron doping (Fig. 7), in spite of the much higher temperature of the FOMT in the latter. This proves that at the silicon-poor composition of sample S3, the magnetoelastic transition at the FOMT (also involving a phase boundary with an incommensurate SDW phase) and the $3f$ moment quenching are actually independent phenomena. Nevertheless, the drop of the $3f$ moment proceeds up to a spinless state of the $3f$ ions at temperatures high enough. This is verified directly by ^{55}Mn NMR well above T_C in a strong applied field whenever applicable, namely in the Mn-richer sample S2 (and, with much lower accuracy, S1), showing a significant fraction of $3f$ sites occupied by Mn ions. The direct detection of a nonmagnetic $3f$ Mn state confirms the initial prediction of a vanishing spin density at the $3f$ sites by band structure calculations [5], later challenged, however, by XMCD [4], thus solving a long-standing controversy.

Besides the majority fraction of "normal" $3f$ Mn atoms that develop itinerant magnetism below T_C, a Mn species with even weaker interactions with the surrounding magnetic ions and preserving its non-magnetic character down to the lowest temperatures, is revealed by the same NMR experiments on Mn-rich compositions. Though minority, such a diamagnetic fraction is sizable ($\approx$0.12 Mn atoms per FU in S2) and ^{55}Mn nuclei therein experience spin fluctuations. It belongs therefore to the magnetic material under examination and not to an undetected (and unprecedented) nonmagnetic Mn impurity phase. Indeed, we are not aware of any nonmagnetic, ionic state of manganese, that are in contrast well documented, e.g., in cobalt, whose Co^{3+} ion exhibits a low-spin (i.e., spinless) ground state in an octahedral crystal field [27,37]. The disproportionation of Mn into high-spin and low-spin species at distinct sites, on the other hand, is possible in intermetallic compounds, including metallic manganese itself (α-Mn) [38], whose Mn-IV atoms exhibit a nearly spinless state [39]. We therefore argue that the diamagnetic Mn state found in these compounds may be driven by a similar spontaneous electronic segregation within the proper Mn-Fe-Si-P phase. To this end, it is worth noting that the Korringa-law behavior $T_1^{-1} \propto T$, obeyed by both ^{55}Mn species above T_C [Fig. 11(b)] and indicating a dominant contribution to their spin-lattice relaxations by band electrons, agrees with the belonging to a metallic phase of the diamagnetic fraction as well. The lack of a significant diamagnetic Mn signal in the Mn-poorer S3 and S4 compounds where no Mn occupancy of $3f$ sites by Mn is expected (and a small one is detected by ZF NMR) indicates that diamagnetic Mn as well occupy $3f$ sites. In this view, the electronic segregation, still to be identified, should involve two slightly different states of the $3f$ ion, weakly magnetic and strictly nonmagnetic, respectively.

The relevance of a diamagnetic Mn fraction at the $3f$ sites for the magnetic and magnetocaloric properties of the materials where it is present in a significant amount is unclear so far. However, it accounts qualitatively for some discrepancies found from the ZF ^{55}Mn NMR spectra of the Mn-richer S2 compound ($x = 1.7$), namely, a $3f$ to $3g$ intensity ratio smaller than expected (Table II) and, on the contrary, a larger estimate for the $3f$ moment by NMR than by neutron scattering (Fig. 3). It is noteworthy that the estimated diamagnetic fraction of sample S2 nearly equals its missing fraction of $3f$ ordered moments. Sample S1 ($x = 1.27$) also shows a significant diamagnetic Mn fraction. Here the $3f$ ZF NMR peak amplitude is in fair agreement with its expected value, but this may be the results of a compensation by off-site Mn atoms spilled over from their preferential $3g$ site, as in sample S4. In the presence of a disproportionation between magnetic and nonmagnetic species at the same crystallographic site, on the other hand, a probe in reciprocal space (neutron scattering) yields the average moment at the site, while a probe in direct space (NMR) selectively probes the moment of each magnetic species. This observation, therefore, qualitatively explains the steeper decrease of the $3f$ ordered moment vs Mn concentration as determined by neutrons with respect to NMR. However, we have no explanation for the opposite relative dependence observed by the two techniques at the $3g$ site, where a moment decrease is detected by NMR only.

V. CONCLUSIONS

In summary, the ubiquitous first-order character of the magnetic transition in Fe_2P-based Mn-Fe-Si-P compounds

is established by ^{55}Mn NMR. The transition is strongly first order, in particular, also at the Mn-rich composition $Mn_{1.7}Fe_{0.25}Si_{0.5}P_{0.5}$, whose macroscopic magnetic and magnetocaloric response approach that of a regular SOMT [1]. However, the latter compound is by no means on the verge of a FOMT-SOMT phase boundary, contrary to the current understanding, and its seeming SOMT is rather the accidental result of a broad distribution of transition temperatures in a blurred magnetoelastic transition [6].

The mixed magnetism of these systems is unambiguously ascribed to the vanishing of the spin polarization at the $3f$ sites in the PM phase, with a very stringent upper limit for the remnant fluctuating $3f$ moment set by the comparison of NMR and magnetization data. The experimental proof of the evolution of $3f$ Mn ions to a truly nonmagnetic state, in partial disagreement with previous conclusions drawn by XMCD, which is yet a more indirect probe of magnetism than NMR [4], is in our view the most important result of this paper. The complete extinction of the $3f$ spin density, however, seems to be attained well above T_C, which indicates that mixed magnetism and the magnetoelastic transitions are partly independent phenomena.

Besides the majority $3f$ Mn atoms exhibiting mixed magnetism, a minority but sizable temperature-independent fraction of diamagnetic manganese is detected by NMR at the $3f$ site in Mn-rich compounds. Although its role in the magnetic properties of these materials is unknown, its occurrence indicates that a subtle electronic segregation mechanism, still to be understood, is at play in these systems.

ACKNOWLEDGMENTS

This work is part of an Industrial Partnership Program IPP I28 of the Stichting voor Fundamenteel Onderzoek der Materie (FOM), which is financially supported by the Nederlandse Organisatie voor Wetenschappelijk Onderzoek (NWO) and cofinanced by BASF Future Business.

[1] N. H. Dung, L. Zhang, Z. Q. Ou, and E. Brück, Appl. Phys. Lett. **99**, 092511 (2011).
[2] N. H. Dung, L. Zhang, Z. Q. Ou, L. Zhao, L. van Eijck, A. M. Mulders, M. Avdeev, E. Suard, N. H. van Dijk, and E. Brück, Phys. Rev. B **86**, 045134 (2012).
[3] X. F. Miao, L. Caron, P. Roy, N. H. Dung, L. Zhang, W. A. Kockelmann, R. A. de Groot, N. H. van Dijk, and E. Brück, Phys. Rev. B **89**, 174429 (2014).
[4] H. Yibole, F. Guillou, L. Caron, E. Jiménez, F. M. F. de Groot, P. Roy, R. de Groot, N. H. van Dijk, and E. Brück, Phys. Rev. B **91**, 014429 (2015).
[5] N. H. Dung, Z. Q. Ou, L. Caron, L. Zhang, D. T. Thanh, G. A. De Wijs, R. A. De Groot, K. H. Buschow, and E. Brück, Adv. Energy Mater. **1**, 1215 (2011).
[6] X. F. Miao, L. Caron, J. Cedervall, P. C. M. Gubbens, P. Dalmas de Réotier, A. Yaouanc, F. Qian, A. R. Wildes, H. Luetkens, A. Amato *et al.*, Phys. Rev. B **94**, 014426 (2016).
[7] P. Jernberg, A. Yousif, L. Häggström, and Y. Andersson, J. Solid State Chem. **53**, 313 (1984).
[8] G. Allodi, R. D. Renzi, K. Zheng, S. Sanna, A. Sidorenko, C. Baumann, L. Righi, F. Orlandi, and G. Calestani, J. Phys.: Condens. Matter **26**, 266004 (2014).
[9] N. V. Thang, H. Yibole, N. H. van Dijk, and E. Brück, J. Alloys Compd. **699**, 633 (2017).
[10] X. Miao, L. Caron, P. Gubbens, A. Yaouanc, P. D. de Réotier, H. Luetkens, A. Amato, N. van Dijk, and E. Brück, J. Sci.: Adv. Mater. Devices **1**, 147 (2016), special issue in memory of Dr. P.E. Brommer.
[11] X. F. Miao, Y. Mitsui, A. I. Dugulan, L. Caron, N. V. Thang, P. Manuel, K. Koyama, K. Takahashi, N. H. van Dijk, and E. Brück, Phys. Rev. B **94**, 094426 (2016).
[12] G. Allodi, A. Banderini, R. De Renzi, and C. Vignali, Rev. Sci. Instrum. **76**, 083911 (2005).
[13] P. C. Riedi, Hyperfine Interact. **49**, 335 (1989).
[14] M. A. Turov and M. P. Petrov, *Nuclear Magnetic Resonance in Ferro- and Antiferromagnets* (Halsted, New York, 1972).
[15] P. Panissod, in *Frontiers in Magnetism of Reduced Dimension Systems*, edited by V. G. Bar'yakthar, P. E. Wigen, and N. A. Lesnik (Springer Netherlands, Dordrecht, 1998), pp. 225–270.
[16] A. M. Portis and R. H. Lindquist, in *Magnetism*, edited by G. T. Rado and H. Suhl (Academic Press, New York, 1965), Vol. IIA.
[17] E. Koster and B. G. Turrell, J. Appl. Phys. **42**, 1314 (1971).
[18] A. J. Freeman and R. E. Watson, in *Magnetism*, edited by G. T. Rado and H. Suhl (Academic Press, New York, 1965), Vol. IIA.
[19] The slight difference in the absolute values of the hyperfine field between samples S3 and S4 is possibly related to the larger amount of misplaced Mn atoms at the $3f$ sites found in S4 (Table II).
[20] J. Barak, D. Fekete, N. Kaplan, and H. Guggenheim, J. Magn. Magn. Mater. **1**, 153 (1975).
[21] A. V. Zalesskii, A. A. Frolov, A. K. Zvezdin, A. A. Gippius, E. N. Morozova, D. F. Khozeevc, A. S. Bush, and V. S. Pokatilov, J. Exp. Theor. Phys. **95**, 101 (2002).
[22] X. Miao, N. Thang, L. Caron, H. Yibole, R. Smith, N. van Dijk, and E. Brück, Scr. Mater. **124**, 129 (2016).
[23] T. Moriya, Prog. Theor. Phys. **16**, 641 (1956).
[24] V. Jaccarino, in *Magnetism*, edited by G. T. Rado and H. Suhl (Academic Press, New York, 1965), Vol. IIA.
[25] A. Abragam, *The Principles of Nuclear Magnetism*, International series of monographs on physics (Clarendon Press, Oxford, 1961).
[26] C. P. Slichter, *Principles of Magnetic Resonance*, Springer series in solid state sciences (Springer-Verlag, Berlin Heidelberg, 1990).
[27] T. Lancaster, S. R. Giblin, G. Allodi, S. Bordignon, M. Mazzani, R. De Renzi, P. G. Freeman, P. J. Baker, F. L. Pratt, P. Babkevich *et al.*, Phys. Rev. B **89**, 020405(R) (2014).
[28] K. Nehrke and M. W. Pieper, Phys. Rev. Lett. **76**, 1936 (1996).
[29] The $\sqrt{3}$ prefactor stems from σ being proportional to the distribution width ΔB_z of the longitudinal field component, $\sigma^2 = (\gamma^2/2\pi)^2\,\Delta B_z^2$. Clearly, $\Delta B^2 = 3\Delta B_z^2$.

[30] T. Kubo, A. Hirai, and H. Abe, J. Phys. Soc. Jpn. **26**, 1094 (1969).
[31] ^{31}P NMR in these samples is the subject of a distinct investigation and will be reported elsewhere.
[32] G. Allodi, R. De Renzi, F. Licci, and M. W. Pieper, Phys. Rev. Lett. **81**, 4736 (1998).
[33] G. Allodi, M. C. Guidi, R. De Renzi, A. Caneiro, and L. Pinsard, Phys. Rev. Lett. **87**, 127206 (2001).
[34] In such a temperature range, the very large linewidth of peak 2 makes a reliable assessment of its position and amplitude, hence a cross-calibration of the amplitudes of the two peaks, impossible.
[35] G. Allodi, M. Bimbi, R. De Renzi, C. Baumann, M. Apostu, R. Suryanarayanan, and A. Revcolevschi, Phys. Rev. B **78**, 064420 (2008).
[36] C. P. Adams, J. W. Lynn, V. N. Smolyaninova, A. Biswas, R. L. Greene, W. Ratcliff, S.-W. Cheong, Y. M. Mukovskii, and D. A. Shulyatev, Phys. Rev. B **70**, 134414 (2004).
[37] G. Allodi, R. De Renzi, S. Agrestini, C. Mazzoli, and M. R. Lees, Phys. Rev. B **83**, 104408 (2011).
[38] D. Hobbs, J. Hafner, and D. Spišák, Phys. Rev. B **68**, 014407 (2003).
[39] H. Yamagata and K. Asayama, J. Phys. Soc. Jpn. **33**, 400 (1972).